Chapter 16

Hyperpolarized Carbon (^{13}C) MRI of the Kidneys: Basic Concept

Cornelius von Morze, Galen D. Reed, Zhen J. Wang, Michael A. Ohliger, and Christoffer Laustsen

Abstract

Existing clinical markers for renal disease are limited. Hyperpolarized (HP) ^{13}C MRI is based on the technology of dissolution dynamic nuclear polarization (DNP) and provides new avenues for imaging kidney structure, function, and most notably, renal metabolism, addressing some of these prior limitations. Changes in kidney structure and function associated with kidney disease can be evaluated using [^{13}C]urea, a metabolically inert tracer. Metabolic changes can be assessed using [1-^{13}C]pyruvate and a range of other rapidly metabolized small molecules, which mainly probe central carbon metabolism. Results from numerous preclinical studies using a variety of these probes demonstrated that this approach holds great potential for monitoring renal disease, although more work is needed to bridge intelligently into clinical studies. Here we introduce the general concept of HP ^{13}C MRI and review the most relevant probes and applications to renal disease, including kidney cancer, diabetic nephropathy and ischemic kidney injury.

This chapter is based upon work from the PARENCHIMA COST Action, a community-driven network funded by the European Cooperation in Science and Technology (COST) program of the European Union, which aims to improve the reproducibility and standardization of renal MRI biomarkers. This introduction chapter is complemented by two separate chapters describing the experimental procedure and data analysis.

Key words Dynamic nuclear polarization, Kidney, Preclinical models, Carbon-13

1 Introduction

While renal MRI has traditionally been limited largely to morphologic depiction of vascular disease and neoplasia, hyperpolarized (HP) ^{13}C MRI supplies new metabolic and/or functional insight that could be valuable for a range of kidney diseases. The high renal delivery of intravenously injected small molecules, which provides extraordinary sensitivity for renal imaging of HP ^{13}C MRI probes, suggests great potential for application of this nascent medical imaging modality to kidney disease.

Andreas Pohlmann and Thoralf Niendorf (eds.), *Preclinical MRI of the Kidney: Methods and Protocols*, Methods in Molecular Biology, vol. 2216, https://doi.org/10.1007/978-1-0716-0978-1_16,

Commonly used clinical markers for kidney disease have significant limitations, especially in the context of early disease. Serum creatinine is frequently utilized as a functional marker, but has a wide reference interval, and the mathematical corrections applied for the estimation of glomerular filtration rate (GFR) are inexact. For example, GFR is unpredictably overestimated in glomerulopathic patients as a result of increased creatinine secretion [1]. Even accurately measured GFR, such as by the "gold standard" inulin clearance, is insensitive to early disease [2]. Blood urea nitrogen (BUN) fluctuates due to factors unrelated to kidney function, such as hydration status and diet. Proteinuria at baseline is a significant risk factor for renal disease, but has poor negative predictive value [3]. In general, clinical markers do not exhibit definitive changes until a significant fraction of kidney function is already lost.

Medical imaging has clear potential to address these limitations by providing localized functional data, but this has yet to be translated on a large scale. Nuclear medicine plays a significant role, with (mercaptoacetyltriglycine) MAG_3 scintigraphy estimated to account for >400,000 renograms per year [4], commonly for evaluation of renal function (often pre- or post-transplant), split function, collecting duct/urinary tract obstruction, renovascular hypertension, and renal artery stenosis. However, nuclear scans typically have relatively poor spatial resolution and lack the rich tissue contrast of MRI. Furthermore, these studies carry the risks of exposure to ionizing radiation. Ultrasound is also commonly used for assessing kidney disease [5], but is generally limited to evaluating advanced damage reflected in alterations in kidney size and shape, and to some extent blood flow. For patients with impaired renal function, iodinated Computer Tomography (CT) contrast media carry an increased risks of acute kidney injury [6]. Gadolinium based MRI contrast media are associated with nephrogenic systemic fibrosis [7].

HP ^{13}C MRI has unique potential for improved, safer clinical imaging studies of renal structure and function, and perhaps most notably offers an unprecedented avenue toward assessing renal metabolism in vivo. Indeed, results of numerous preclinical studies conducted to date, as summarized below, show the clear potential of this new approach to fill pressing unmet clinical needs for improved markers of various diseases affecting the kidneys, both malignant and nonmalignant. More preclinical work with realistic renal disease models is, however, needed in order to bridge effectively into clinical studies.

This introduction chapter is complemented by two separate chapters describing the experimental procedure and data analysis, which are part of this book.

This chapter is part of the book Pohlmann A, Niendorf T (eds) (2020) Preclinical MRI of the Kidney—Methods and Protocols. Springer, New York.

2 Measurement Concept

2.1 Basic Concept of HP ^{13}C MRI

HP ^{13}C MRI is based on a transient enhancement of the nuclear magnetism of ^{13}C-enriched liquids, by up to five orders of magnitude over states readily attainable in a clinical MRI magnet, thereby offsetting the limitation of poor sensitivity that previously hampered in vivo ^{13}C MRI. Although multiple alternate approaches exist for producing HP material, the method of dissolution dynamic nuclear polarization (DNP) [8] provides an especially robust avenue for hyperpolarizing a wide variety of ^{13}C-labeled substrates, using commercially available instruments. In this approach, the ^{13}C substrate is first prepolarized in a separate magnet at low temperature (*see* **Note 1**), primarily through microwave irradiation applied near the electron paramagnetic resonance (EPR) frequency in the presence of a stable organic free radical (aka electron paramagnetic agent or EPA, usually a trityl radical) (*see* **Note 2**). Following a period of polarization buildup, the solid sample is rapidly dissolved into a liquid state where it temporarily maintains its hyperpolarization, and is quickly transferred to the MRI scanner for intravenous injection and imaging (*see* **Note 3**). The overall process is illustrated in Fig. 1. The transient hyperpolarized state persists for a period of time determined by the substrate's T_1 relaxation time, an exponential time constant governing the rate of decay of polarization (*see* **Note 4**). Inverse scaling of T_1 with molecular size limits the scope of applicable probes to small molecules, with labels preferably located distal to bonded hydrogen atoms, which can destroy the ^{13}C magnetization via ^{13}C-^{1}H dipolar coupling (*see* **Note 5**). During the decay period, ^{13}C MRI data is collected, capitalizing on the sensitivity enhancement afforded by hyperpolarization. Specific methods for data acquisition and processing of HP ^{13}C MRI data are described in the relevant sections to follow.

2.2 Renal Functional and Metabolic Investigations Using HP ^{13}C MRI

HP ^{13}C MRI offers many new possibilities for renal functional and metabolic investigations. Dynamic images of the real-time delivery of metabolically inert tracers such as ^{13}C urea from arterial vasculature to the kidneys can be used to quantify renal function. Real-time in vivo processing of metabolically active HP probes by the kidneys can be tracked by spectroscopic imaging, which yields separate images of injected tracer(s) and their downstream metabolic product(s) based on chemical shift differences. Notably, multiple probes can also be simultaneously copolarized to yield multiparametric data sets [9], for example spanning both renal functional and metabolic parameters. In this section, we review the most promising HP ^{13}C MRI probes of renal function/metabolism proposed to date, and the relevant associated principles. These probes and their metabolic pathways are illustrated in Fig. 2.

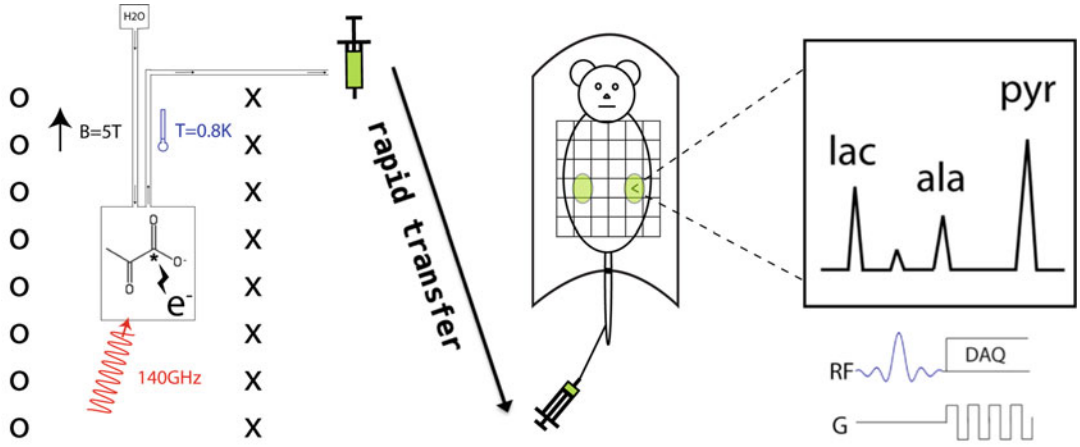

Fig. 1 Illustration of the process of HP ^{13}C MRI via dissolution dynamic nuclear polarization. The agent (e.g., [1-^{13}C]pyruvate) is mixed with the EPA and cooled to 0.8 K in a magnetic field of 5 T, then irradiated at 140GHz to transfer polarization from unpaired electrons in the EPA to the ^{13}C nuclei. The sample is then rapidly dissolved and transferred to the MRI scanner for intravenous injection and MR imaging

2.2.1 [^{13}C]Urea

The key osmolyte and metabolic end product urea was one of the first ^{13}C-labeled molecules to be hyperpolarized ($T_1 = 45$ s at 3 T) [8] and imaged in vivo [10], and high quality dynamic images of the kidneys and the feeding arterial vasculature can readily be generated [11–13]. Quantitative estimates of renal function require dynamic measurements from both the renal parenchyma and arterial vasculature [11, 14]. Urea is largely reabsorbed by urea transporters (UTs) expressed at the inner medullary collecting ducts (IMCD), and accordingly renal imaging shows distinct modulation by hydration state [13, 15], based on differential action of vasopressin. Despite this significant reabsorption, it has been suggested that urea can also be used to estimate glomerular filtration rate (GFR) [14], based on the first-order transfer coefficient between arterial vasculature and renal parenchyma. Secondary labeling of [^{13}C]urea with $^{15}N_2$ is helpful in terms of prolonging both T_1 (at low magnetic fields only) [16] and T_2 relaxation times [12] of urea, with the latter factor allowing imaging rat kidneys at spatial resolutions approaching 1 mm isotropic (using refocused image acquisition) [13]. Furthermore, relaxation mapping shows great promise for improved contrast between the individual kidney compartments and various functional states [12, 13, 17]. Urea is distinguished by an exceptionally good safety profile among medical imaging contrast agents, even in patients with reduced kidney function, and therefore has potential for clinical translation for imaging patients with kidney diseases.

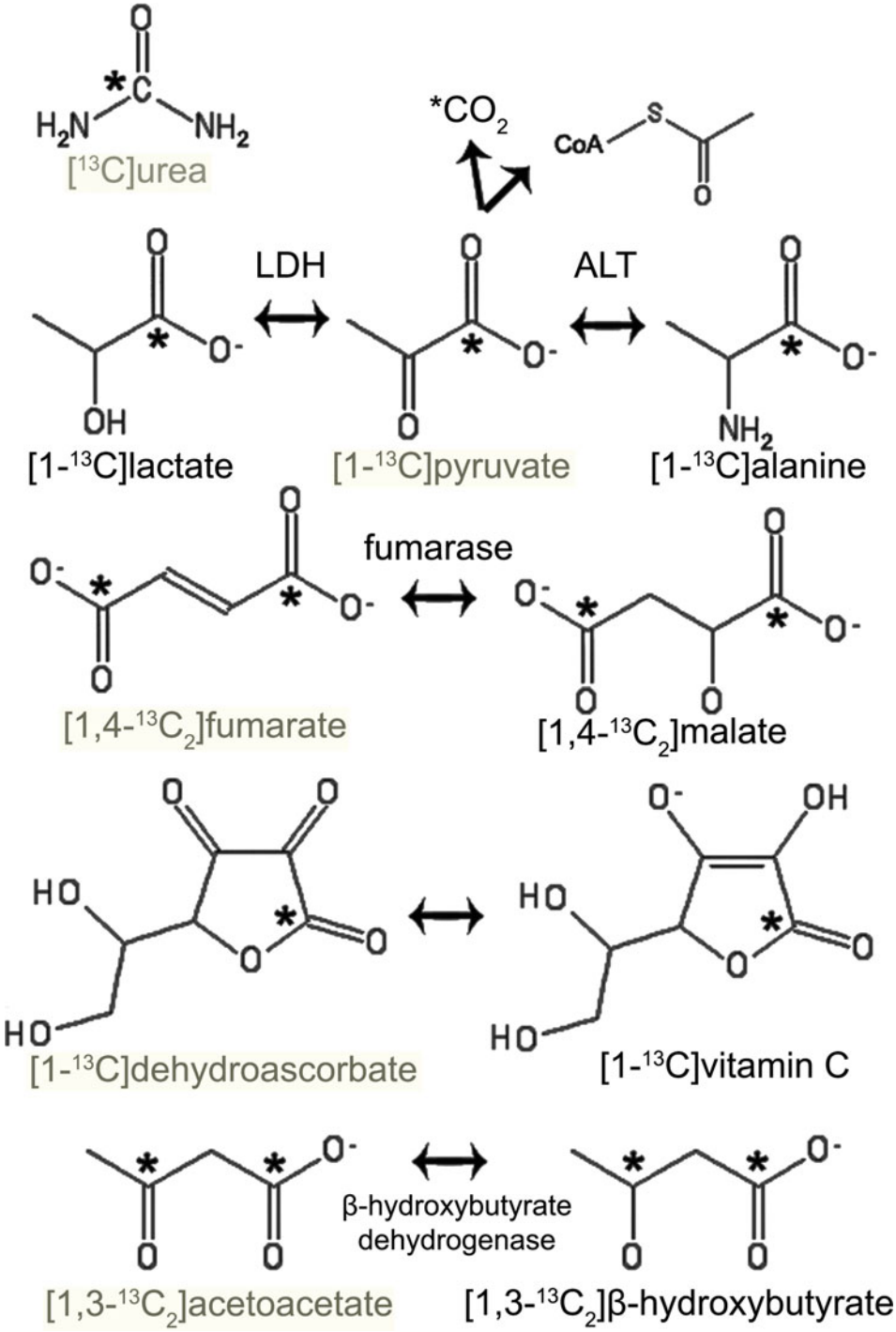

Fig. 2 HP ^{13}C MRI probes of interest for monitoring renal disease, and the associated metabolic conversions (if any). Positions of the ^{13}C labels are indicated by stars

2.2.2 [1-^{13}C]Pyruvate

Pyruvate, the end product of glycolysis and key metabolic intermediate, is the most widely studied ^{13}C probe, in C_1-labeled form (T_1 = 60s at 3 T) [18]. In the kidneys, its interconversions with lactate (via lactate dehydrogenase, LDH) and alanine (via alanine transaminase, ALT), as well as its decarboxylation yielding [^{13}C] bicarbonate (via pyruvate dehydrogenase or PDH) can readily be tracked by spectroscopic imaging. The extent of metabolic conversion observed reflects a complex series of biophysical processes, including vascular delivery, cellular uptake (via monocarboxylate transporters), and finally enzymatic conversion, which in turn may be influenced by multiple factors. For the conversion via LDH, the lactate pool size is especially important [19, 20]. For quantitative comparison among subjects, all of these factors are usually grouped into simple parameters such as metabolite area-under-the-curve (AUC) ratios or related apparent first-order conversion rates (e.g., $k_{pyruvate\text{-}to\text{-}lactate}$ or k_{pl}) [21, 22], derived from a series of dynamic spectroscopic imaging data. From a metabolic perspective, while the conversion to bicarbonate is clearly a net flux, the conversions to lactate and alanine via the respective bidirectional, highly active enzymes appear to represent largely isotopic exchange fluxes into the respective product metabolite pools [19, 20, 23]. Because of the high bidirectional activity of LDH (which is restricted to cytoplasm), the ratio of lactate to pyruvate has frequently been interpreted as a marker for the cytosolic free NADH/NAD$^+$ ratio [24]. This suggests that the conversion of HP pyruvate to lactate is driven by this NAD(H) redox state, a parameter that is fundamentally inter-connected with numerous related biochemical reactions.

2.2.3 [1,4-$^{13}C_2$]Fumarate

Cellular uptake of injected fumarate, a tricarboxylic acid (TCA) cycle intermediate, is ordinarily highly restricted on the timescale of HP experiments, due to its dicarboxylate structure. Compromise of the cellular membrane (e.g., due to necrosis) allows access of injected HP [1,4-$^{13}C_2$]fumarate (a singlet due to molecular symmetry, with T_1 = 58 s at 3 T) [25] to cellular fumarase, and consequently detectable conversion of product HP [1,4-$^{13}C_2$] malate. Thus, HP fumarate has been investigated as a specific marker of cellular necrosis with potentially significant applicability to detection of renal tubular necrosis [26].

2.2.4 [1-^{13}C] Dehydroascorbate

HP [1-^{13}C]dehydroascorbate (T_1 = 56 s at 3 T) [27, 28] can be used to probe oxidative stress in a direct manner. Vitamin C, a key physiologic antioxidant, exists in a NADP(H)-mediated equilibrium with its oxidized form, dehydroascorbate (DHA). Conversion of injected HP [1-^{13}C]DHA, which is rapidly taken up by glucose transporters, to [1-^{13}C]vitamin C is detectable in vivo. The observed extent of conversion of HP DHA to vitamin C, a reaction whose reducing power is likely mostly derived from reduced glutathione (GSH), is attenuated by oxidative stress.

2.2.5 [^{13}C]Acetoacetate

The ketone body acetoacetate, a universal oxidative fuel, rapidly interconverts with its reduced form, beta-hydroxybutyrate, in mitochondria via beta-hydroxybutyrate dehydrogenase. In analogy with lactate/pyruvate, the BOHB–AcAc ratio has frequently been interpreted as a marker of the free mitochondrial NADH–NAD$^+$ ratio, suggesting an analogous interpretation of conversion of HP acetoacetate [29, 30] as being driven by the mitochondrial NAD(H) redox state. Metabolic conversion of injected [1,3-$^{13}C_2$]acetoacetate (58 s at 3 T, C_1 position) can be detected in rat kidney in vivo (via the C_1 label) [29], suggesting applicability of this new probe to interrogate mitochondrial-driven kidney disease.

3 Overview of Applications

3.1 Kidney Cancer

Multiple studies have reported elevated conversion of HP [1-^{13}C]pyruvate to [1-^{13}C]lactate and rapid export of [1-^{13}C]lactate in renal cell carcinoma (RCC), in both RCC cells ex vivo [31–33] and in vivo in mice orthotopically implanted with human RCC cells [34]. These findings suggest that HP [1-^{13}C]pyruvate MRI could have clinical value for improved characterization of kidney cancer in patients. Moreover, a recent study showed that HP [1-^{13}C]pyruvate MRI could be used to predict RCC treatment response to mTOR inhibition, which varies greatly among individual patients, thus potentially informing treatment decisions [35].

3.2 Diabetic Nephropathy

Diabetes results in profound shifts in central carbon metabolism, directly shifting several pathways accessible to HP ^{13}C MRI. Although diabetes is detectable using relatively simple testing, sustained hyperglycemia over time leads to serious end-organ complications including diabetic nephropathy, a significant source of morbidity, the detection/prediction of which is a difficult clinical problem where HP ^{13}C MRI could be valuable. Though cancer has been the main focus of the HP ^{13}C MRI community, several recent studies have reported differences in renal HP ^{13}C signals detected in type 1 and type 2 diabetes models as compared to normal controls, based on multiple HP probes including [1-^{13}C]pyruvate [23, 36, 37], [^{13}C]urea [38, 39], and [1-^{13}C]DHA [40]. Not surprisingly, standard antidiabetic agents including insulin and metformin have been found to induce large renal HP signal changes as well [29, 41, 42]. Renal HP lactate levels are attenuated with hyperbaric [43] and antioxidant treatment [44] in diabetic rats. HP [^{13}C]acetate has so far failed to show any significant metabolic change associated with the diabetic kidney [45]. Further work is needed in animal models of frank diabetic nephropathy, which may display changes additive to the fundamental metabolic shifts observed in diabetes, to address this important clinical problem.

3.3 Ischemic Kidney Injury

Effective detection of acute kidney injury (AKI) is an unresolved clinical problem especially affecting hospitalized patients. Rapid treatment of AKI is critical but is impeded by existing clinical indicators which are poor in diagnosing early AKI. Several studies of models of ischemia reperfusion injury (i.e., unilateral renal artery clamp) have shown clear effects of AKI on renal HP ^{13}C MRI using [^{13}C]urea [46, 47], pyruvate [48], and [1-^{13}C]pyruvate–[1-^{13}C] DHA combination [49], and fumarate [50]. However, these relatively simple models likely do not reflect the etiology of ischemic injuries more frequently encountered in patients, such as those resulting from atherosclerotic disease. Further work using more realistic models of ischemic kidney injury is needed to answer, for example, the important question of predicting treatment response in renal artery stenosis. Finally, HP [1,4-$^{13}C_2$]fumarate has also been investigated as a probe of tissue necrosis in a toxic folic acid model of acute tubular necrosis (ATN) [26]. A nonzero urinary fumarase activity could potentially be used as a clinical indicator for a hyperpolarized fumarate examination to investigate the extent and the origin of the renal damage [50].

4 Notes

1. The state-of-the-art GE SPINLab polarizer operates at 5 T and a temperature of 0.8 K. Microwave irradiation is applied near the EPR frequency corresponding to this magnetic field (~140 GHz), with a typical power of ~20 mW. A buildup time of ~3 h is typically required.
2. Urea and many other agents including fumarate and acetoacetate require the addition of a glassing agent such as glycerol or DMSO to prevent crystallization upon freezing, which impedes the polarization process.
3. The ^{13}C concentration is made as high as possible in the starting material (in the molar range), facilitating efficient polarization, but the concentration typically drops >10-fold on dissolution. In contrast, the concentration of the radical is only ~15 mM in the starting material.
4. The T_1 exponential decay constant of HP ^{13}C probe is directly proportional to its "half-life," by a factor of ln 2 (i.e., $t_{1/2} = 0.69 \times T_1$).
5. T_1 values of 30–60 s are typical for the most useful probes, and T_1 values are magnetic field- and temperature-dependent.

Acknowledgments

Grant support from National Institutes of Health (NIH) K01DK099451 is gratefully acknowledged.
This chapter is based upon work from COST Action PARENCHIMA, supported by European Cooperation in Science and Technology (COST). COST (www.cost.eu) is a funding agency for research and innovation networks. COST Actions help connect research initiatives across Europe and enable scientists to enrich their ideas by sharing them with their peers. This boosts their research, career, and innovation.
PARENCHIMA (renalmri.org) is a community-driven Action in the COST program of the European Union, which unites more than 200 experts in renal MRI from 30 countries with the aim to improve the reproducibility and standardization of renal MRI biomarkers.

References

1. Shemesh O, Golbetz H, Kriss JP, Myers BD (1985) Limitations of creatinine as a filtration marker in glomerulopathic patients. Kidney Int 28:830–838
2. Metcalfe W (2007) How does early chronic kidney disease progress? A background paper prepared for the UK Consensus Conference on early chronic kidney disease. Nephrol Dial Transplant 22(Suppl 9):ix26–ix30. https://doi.org/10.1093/ndt/gfm446
3. Ishani A, Grandits GA, Grimm RH, Svendsen KH, Collins AJ, Prineas RJ, Neaton JD (2006) Association of single measurements of dipstick proteinuria, estimated glomerular filtration rate, and hematocrit with 25-year incidence of end-stage renal disease in the multiple risk factor intervention trial. J Am Soc Nephrol 17:1444–1452. https://doi.org/10.1681/ASN.2005091012
4. Esteves FP, Taylor A, Manatunga A, Folks RD, Krishnan M, Garcia EV (2006) 99mTc-MAG3 renography: normal values for MAG3 clearance and curve parameters, excretory parameters, and residual urine volume. AJR Am J Roentgenol 187:W610–W617. https://doi.org/10.2214/AJR.05.1550
5. O'Neill WC (2014) Renal relevant radiology: use of ultrasound in kidney disease and nephrology procedures. Clin J Am Soc Nephrol 9:373–381. https://doi.org/10.2215/CJN.03170313
6. PA MC, Stacul F, Becker CR, Adam A, Lameire N, Tumlin JA, Davidson CJ, CIN Consensus Working Panel (2006) Contrast-induced nephropathy (CIN) consensus working panel: executive summary. Rev Cardiovasc Med 7:177–197
7. Kuo PH, Kanal E, Abu-Alfa AK, Cowper SE (2007) Gadolinium-based MR contrast agents and nephrogenic systemic fibrosis. Radiology 242:647–649. https://doi.org/10.1148/radiol.2423061640
8. Ardenkjaer-Larsen JH, Fridlund B, Gram A, Hansson G, Hansson L, Lerche MH, Servin R, Thaning M, Golman K (2003) Increase in signal-to-noise ratio of > 10,000 times in liquid-state NMR. Proc Natl Acad Sci U S A 100:10158–10163. https://doi.org/10.1073/pnas.1733835100
9. Wilson DM, Keshari KR, Larson PEZ, Chen AP, Hu S, Van Criekinge M, Bok R, Nelson SJ, Macdonald JM, Vigneron DB, Kurhanewicz J (2010) Multi-compound polarization by DNP allows simultaneous assessment of multiple enzymatic activities in vivo. J Magn Reson 205:141–147. https://doi.org/10.1016/j.jmr.2010.04.012
10. Golman K, Ardenkjaer-Larsen JH, Petersson JS, Månsson S, Leunbach I (2003) Molecular imaging with endogenous substances. Proc Natl Acad Sci U S A 100:10435–10439. https://doi.org/10.1073/pnas.1733836100
11. von Morze C, Larson PEZ, Hu S, Keshari K, Wilson DM, Ardenkjaer-Larsen JH, Goga A, Bok R, Kurhanewicz J, Vigneron DB (2011) Imaging of blood flow using hyperpolarized [C-13] urea in preclinical cancer models. J

Magn Reson Imaging 33:692–697. https://doi.org/10.1002/jmri.22484

12. Reed GD, von Morze C, Bok R, Koelsch BL, Van Criekinge M, Smith KJ, Shang H, Larson PEZ, Kurhanewicz J, Vigneron DB (2014) High resolution (13)C MRI with hyperpolarized urea: in vivo T(2) mapping and (15)N labeling effects. IEEE Trans Med Imaging 33:362–371. https://doi.org/10.1109/TMI.2013.2285120
13. Reed GD, von Morze C, Verkman AS, Koelsch BL, Chaumeil MM, Lustig M, Ronen SM, Bok RA, Sands JM, Larson PEZ, Wang ZJ, Larsen JHA, Kurhanewicz J, Vigneron DB (2016) Imaging renal urea handling in rats at millimeter resolution using hyperpolarized magnetic resonance relaxometry. Tomography 2:125–135. https://doi.org/10.18383/j.tom.2016.00127
14. Østergaard Mariager C, Nielsen PM, Qi H, Schroeder M, Bertelsen LB, Laustsen C (2017) Can hyperpolarized 13C-urea be used to assess glomerular filtration rate? A retrospective study. Tomography 3:146–152. https://doi.org/10.18383/j.tom.2017.00010
15. von Morze C, Bok RA, Sands JM, Kurhanewicz J, Vigneron DB (2012) Monitoring urea transport in rat kidney in vivo using hyperpolarized C-13 magnetic resonance imaging. Am J Physiol Renal Physiol 302:F1658–F1662. https://doi.org/10.1152/ajprenal.00640.2011
16. Chiavazza E, Kubala E, Gringeri CV, Düwel S, Durst M, Schulte RF, Menzel MI (2013) Earth's magnetic field enabled scalar coupling relaxation of 13C nuclei bound to fast-relaxing quadrupolar 14N in amide groups. J Magn Reson 227:35–38. https://doi.org/10.1016/j.jmr.2012.11.016
17. Laustsen C, Stokholm Nørlinger T, Christoffer Hansen D, Qi H, Mose Nielsen P, Bonde Bertelsen L, Henrik Ardenkjaer-Larsen J, Stødkilde Jørgensen H (2016) Hyperpolarized 13C urea relaxation mechanism reveals renal changes in diabetic nephropathy. Magn Reson Med 75:515–518. https://doi.org/10.1002/mrm.26036
18. Golman K, in 't Zandt R, Thaning M (2006) Real-time metabolic imaging. Proc Natl Acad Sci U S A 103:11270–11275. https://doi.org/10.1073/pnas.0601319103
19. Day SE, Kettunen MI, Gallagher FA, Hu D-E, Lerche M, Wolber J, Golman K, Ardenkjaer-Larsen JH, Brindle KM (2007) Detecting tumor response to treatment using hyperpolarized 13C magnetic resonance imaging and spectroscopy. Nat Med 13:1382–1387. https://doi.org/10.1038/nm1650
20. Hurd RE, Spielman D, Josan S, Yen Y-F, Pfefferbaum A, Mayer D (2013) Exchange-linked dissolution agents in dissolution-DNP (13)C metabolic imaging. Magn Reson Med 70:936–942. https://doi.org/10.1002/mrm.24544
21. Hill DK, Orton MR, Mariotti E, Boult JKR, Panek R, Jafar M, Parkes HG, Jamin Y, Miniotis MF, Al-Saffar NMS, Beloueche-Babari M, Robinson SP, Leach MO, Chung Y-L, Eykyn TR (2013) Model free approach to kinetic analysis of real-time hyperpolarized 13C magnetic resonance spectroscopy data. PLoS One 8:e71996. https://doi.org/10.1371/journal.pone.0071996
22. Daniels CJ, McLean MA, Schulte RF, Robb FJ, Gill AB, McGlashan N, Graves MJ, Schwaiger M, Lomas DJ, Brindle KM, Gallagher FA (2016) A comparison of quantitative methods for clinical imaging with hyperpolarized (13)C-pyruvate. NMR Biomed 29:387–399. https://doi.org/10.1002/nbm.3468
23. von Morze C, Allu PKR, Chang GY, Marco-Rius I, Milshteyn E, Wang ZJ, Ohliger MA, Gleason CE, Kurhanewicz J, Vigneron DB, Pearce D (2018) Non-invasive detection of divergent metabolic signals in insulin deficiency vs. insulin resistance in vivo. Sci Rep 8:2088. https://doi.org/10.1038/s41598-018-20264-w
24. Williamson D, Lund P, Krebs H (1967) Redox state of free nicotinamide-adenine dinucleotide in cytoplasm and mitochondria of rat liver. Biochem J 103:514–527
25. Gallagher FA, Kettunen MI, Hu D-E, Jensen PR, I' nt Zandt R, Karlsson M, Gisselsson A, Nelson SK, Witney TH, Bohndiek SE, Hansson G, Peitersen T, Lerche MH, Brindle KM (2009) Production of hyperpolarized [1,4-13C2]malate from [1,4-13C2]fumarate is a marker of cell necrosis and treatment response in tumors. Proc Natl Acad Sci U S A 106:19801–19806. https://doi.org/10.1073/pnas.0911447106
26. Clatworthy MR, Kettunen MI, Hu D-E, Mathews RJ, Witney TH, Kennedy BWC, Bohndiek SE, Gallagher FA, Jarvis LB, Smith KGC, Brindle KM (2012) Magnetic resonance imaging with hyperpolarized [1,4-(13)C2]fumarate allows detection of early renal acute tubular necrosis. Proc Natl Acad Sci U S A 109:13374–13379. https://doi.org/10.1073/pnas.1205539109
27. Keshari KR, Kurhanewicz J, Bok R, Larson PEZ, Vigneron DB, Wilson DM (2011) Hyperpolarized 13C dehydroascorbate as an endogenous redox sensor for in vivo metabolic

imaging. Proc Natl Acad Sci U S A 108:18606–18611. https://doi.org/10.1073/pnas.1106920108

28. Bohndiek SE, Kettunen MI, Hu D-E, Kennedy BWC, Boren J, Gallagher FA, Brindle KM (2011) Hyperpolarized [1-13C]-ascorbic and dehydroascorbic acid: vitamin C as a probe for imaging redox status in vivo. J Am Chem Soc 133:11795–11801. https://doi.org/10.1021/ja2045925
29. von Morze C, Ohliger MA, Marco-Rius I, Wilson DM, Flavell RR, Pearce D, Vigneron DB, Kurhanewicz J, Wang ZJ (2018) Direct assessment of renal mitochondrial redox state using hyperpolarized 13 C-acetoacetate. Magn Reson Med 79(4):1862–1869. https://doi.org/10.1002/mrm.27054
30. Miller JJ, Ball DR, Lau AZ, Tyler DJ (2018) Hyperpolarized ketone body metabolism in the rat heart. NMR Biomed 31:e3912. https://doi.org/10.1002/nbm.3912
31. Keshari KR, Sriram R, Koelsch BL, Van Criekinge M, Wilson DM, Kurhanewicz J, Wang ZJ (2013) Hyperpolarized 13C-pyruvate magnetic resonance reveals rapid lactate export in metastatic renal cell carcinomas. Cancer Res 73:529–538. https://doi.org/10.1158/0008-5472.CAN-12-3461
32. Sriram R, Van Criekinge M, Hansen A, Wang ZJ, Vigneron DB, Wilson DM, Keshari KR, Kurhanewicz J (2015) Real-time measurement of hyperpolarized lactate production and efflux as a biomarker of tumor aggressiveness in an MR compatible 3D cell culture bioreactor. NMR Biomed 28:1141–1149. https://doi.org/10.1002/nbm.3354
33. Sriram R, Van Criekinge M, Delos Santos J, Keshari KR, Wilson DM, Peehl D, Kurhanewicz J, Wang ZJ (2016) Non-invasive differentiation of benign renal tumors from clear cell renal cell carcinomas using clinically translatable hyperpolarized 13C pyruvate magnetic resonance. Tomography 2:35–42. https://doi.org/10.18383/j.tom.2016.00106
34. Sriram R, Gordon J, Baligand C, Ahamed F, Delos Santos J, Qin H, Bok RA, Vigneron DB, Kurhanewicz J, Larson PEZ, Wang ZJ (2018) Non-invasive assessment of lactate production and compartmentalization in renal cell carcinomas using hyperpolarized 13C pyruvate MRI. Cancers (Basel) 10:313. https://doi.org/10.3390/cancers10090313
35. Dong Y, Eskandari R, Ray C, Granlund KL, Dos Santos-Cunha L, Miloushev VZ, Tee SS, Jeong S, Aras O, Chen Y-B, Cheng EH, Hsieh JJ, Keshari KR (2019) Hyperpolarized MRI visualizes Warburg effects and predicts treatment response to mTOR inhibitors in patient-derived ccRCC xenograft models. Cancer Res 79(1):242–250. https://doi.org/10.1158/0008-5472.CAN-18-2231
36. Laustsen C, Østergaard JA, Lauritzen MH, Nørregaard R, Bowen S, Søgaard LV, Flyvbjerg A, Pedersen M, Ardenkjaer-Larsen JH (2013) Assessment of early diabetic renal changes with hyperpolarized [1-13C]pyruvate. Diabetes Metab Res Rev 29:125–129. https://doi.org/10.1002/dmrr.2370
37. von Morze C, Chang GY, Larson PE, Shang H, Allu PK, Bok RA, Crane JC, Olson MP, Tan CT, Marco-Rius I, Nelson SJ, Kurhanewicz J, Pearce D, Vigneron DB (2017) Detection of localized changes in the metabolism of hyperpolarized gluconeogenic precursors 13C-lactate and 13C-pyruvate in the kidneys and liver. Magn Reson Med 77(4):1429–1437
38. Qi H, Nørlinger TS, Nielsen PM, Bertelsen LB, Mikkelsen E, Xu Y, Stødkilde Jørgensen H, Laustsen C (2016) Early diabetic kidney maintains the corticomedullary urea and sodium gradient. Physiol Rep 4:e12714. https://doi.org/10.14814/phy2.12714
39. Bertelsen LB, Nielsen PM, Qi H, Nørlinger TS, Zhang X, Stødkilde Jørgensen H, Laustsen C (2017) Diabetes induced renal urea transport alterations assessed with 3D hyperpolarized 13 C,15 N-urea. Magn Reson Med 77:1650–1655. https://doi.org/10.1002/mrm.26256
40. Keshari KR, Wilson DM, Sai V, Bok R, Jen K-Y, Larson P, Van Criekinge M, Kurhanewicz J, Wang ZJ (2015) Noninvasive in vivo imaging of diabetes-induced renal oxidative stress and response to therapy using hyperpolarized 13C dehydroascorbate magnetic resonance. Diabetes 64:344–352. https://doi.org/10.2337/db13-1829
41. Laustsen C, Lipsø K, Østergaard JA, Nørregaard R, Flyvbjerg A, Pedersen M, Palm F, Ardenkjaer-Larsen JH (2014) Insufficient insulin administration to diabetic rats increases substrate utilization and maintains lactate production in the kidney. Physiol Rep 2:e12233. https://doi.org/10.14814/phy2.12233
42. Qi H, Nielsen PM, Schroeder M, Bertelsen LB, Palm F, Laustsen C (2018) Acute renal metabolic effect of metformin assessed with hyperpolarised MRI in rats. Diabetologia 61:445–454. https://doi.org/10.1007/s00125-017-4445-6
43. Nørlinger TS, Nielsen PM, Qi H, Mikkelsen E, Hansen K, Schmidt NH, Pedersen M, Agger P, Palm F, Laustsen C (2017) Hyperbaric oxygen therapy reduces renal lactate production.

Physiol Rep 5:e13217. https://doi.org/10.14814/phy2.13217

44. Laustsen C, Nielsen PM, Nørlinger TS, Qi H, Pedersen UK, Bertelsen LB, Østergaard JA, Flyvbjerg A, Ardenkjaer-Larsen JH, Palm F, Stødkilde Jørgensen H (2017) Antioxidant treatment attenuates lactate production in diabetic nephropathy. Am J Physiol Renal Physiol 312:F192–F199. https://doi.org/10.1152/ajprenal.00148.2016
45. Koellisch U, Laustsen C, Nørlinger TS, Østergaard JA, Flyvbjerg A, Gringeri CV, Menzel MI, Schulte RF, Haase A, Stødkilde Jørgensen H (2015) Investigation of metabolic changes in STZ-induced diabetic rats with hyperpolarized [1-13C]acetate. Physiol Rep 3:e12474. https://doi.org/10.14814/phy2.12474
46. Nielsen PM, Szocska Hansen ES, Nørlinger TS, Nørregaard R, Bonde Bertelsen L, Stødkilde Jørgensen H, Laustsen C (2016) Renal ischemia and reperfusion assessment with three-dimensional hyperpolarized 13 C,15 N2-urea. Magn Reson Med 76:1524–1530. https://doi.org/10.1002/mrm.26377
47. Mariager CØ, Nielsen PM, Qi H, Ringgaard S, Laustsen C (2018) Hyperpolarized 13 C,15 N2 -urea T2 relaxation changes in acute kidney injury. Magn Reson Med 80:696–702. https://doi.org/10.1002/mrm.27050
48. Nielsen PM, Laustsen C, Bertelsen LB, Qi H, Mikkelsen E, Kristensen MLV, Nørregaard R, Stødkilde Jørgensen H (2017) In situ lactate dehydrogenase activity: a novel renal cortical imaging biomarker of tubular injury? Am J Physiol Renal Physiol 312:F465–F473. https://doi.org/10.1152/ajprenal.00561.2015
49. Baligand C, Qin H, True-Yasaki A, Gordon JW, von Morze C, Delos Santos J, Wilson DM, Raffai R, Cowley PM, Baker AJ, Kurhanewicz J, Lovett DH, Wang ZJ (2017) Hyperpolarized C-13 magnetic resonance evaluation of renal ischemia reperfusion injury in a murine model. NMR Biomed 30(10). https://doi.org/10.1002/nbm.3765
50. Nielsen PM, Eldirdiri A, Bertelsen LB, Jørgensen HS, Ardenkjaer-Larsen JH, Laustsen C (2017) Fumarase activity: an in vivo and in vitro biomarker for acute kidney injury. Sci Rep 7:40812. https://doi.org/10.1038/srep40812